Performance Analysis of Internally Coded Time-Hopping Coherent Ultrashort Light Pulse CDMA Scheme in Fiber-Optic Communication Systems

Foroogh S. Tabataba, Sahar M. Aghajanzadeh, Masoumeh Nasiri-Kenari, *Member, IEEE*, and Mahdi Karimi

***Abstract*—We consider an internally coded time-hopping coherent ultrashort light pulse code division multiple access scheme (TH-CULP CDMA) and analyze its performance in the fiber-optic communication systems. This system combines the TH and CULP CDMA techniques and exploits the advantages of both. In our method, each bit time interval is divided into N_s frames, and the spectral phase-coded pulse is transmitted in one of these frames. Two exclusive PN sequences are assigned to each user. One is added to a superorthogonal convolutional encoder output to select the transmission frame, and the other is used to encode the phase of the ultrashort pulse in the spectral domain. We evaluate the bit error rate (BER) of the system considering the effects of the multiple access interference (MAI) and thermal noise for both soft and hard decoders. The BER is evaluated using both the Chernoff bound and saddle point approximation. We compare the performance of our proposed system with that of the conventional CULP CDMA system. The numerical results indicate that for the same bit rate and processing gain, the performance of our proposed system (TH-CULP CDMA) is substantially better than that of the conventional CULP CDMA system. In addition, we observe that the hard decoder has a better performance at large number of users compared to the soft decoder.**

***Index Terms*—Coherent ultrashort light pulse (CULP), femtosecond code division multiple access (CDMA), optical CDMA (OCDMA), saddle point approximation, spectral phase encoding (SPE), superorthogonal code, time hopping (TH).**

I. Introduction

FUTURE all-optical networks require techniques to support a large number of simultaneous users demanding voice, video, and data services. Optical code division multiple access (OCDMA) systems have special features which make them suitable for this purpose. These systems exploit the advantages of both an optical communication, such as simplicity, minimum access delay, high throughput, and large bandwidth (leading to high bit rate), and a CDMA technique, such as internal interference rejection capability (which suppresses a narrowband interference) and high security (which is due to the low power spectral density). In an OCDMA system, signals of all transmitters overlap in both the time and frequency domains, and the users are distinguished by their dedicated signature sequences. Therefore, these systems can have higher bandwidth efficiency and flexibility compared to the other multiple access systems.

Several different schemes can be used in OCDMA systems [1]–[9]. They are classified as coherent or incoherent schemes depending on whether or not the encoding and decoding processes make use of a coherent light source. Coherent schemes [1]–[4] manipulate the field of the light pulses by altering its phase, and in these schemes, bipolar spreading codes such as m-sequences, pseudonoise sequences, and Gold codes [12] are used. Incoherent schemes [5], [6] disregard the coherence and utilize the power of the optical signal. Incoherent systems are regarded as more practical because of their lower complexity. On the other hand, the coherent systems achieve better performance than the incoherent ones [10].

One of the earliest coherent techniques, which was proposed during late 1980s, is coherent ultrashort light pulse CDMA (CULP CDMA) or femtosecond CDMA [1]. The performance of this system has been evaluated in [1], with the assumptions of a random binary spreading sequence and an ideal ultrafast photodetector, which is able of outputting the instantaneous power of the pulse. Some recently invented and developed optical devices, such as erbium-doped fiber amplifiers, arrayed-waveguide gratings, superstructured fiber Bragg gratings, semiconductor mode-locked lasers, and finally, all-optical threshold devices, will undoubtedly help the development of this technique in the near future [7]–[9].

Similar to other multiple access systems, the success of the system operation depends on the effective reduction of bit error rate (BER) or, equivalently, increasing the number of users. Channel error correcting is an appropriate technique for this purpose. In most of the previously employed channel coding methods, error-correcting codes are externally applied to the CDMA link [11]–[15]. A disadvantage of an externally coded fiber-optic CDMA scheme is the required extra bandwidth expansion compared to the uncoded system. In order to mitigate the above inefficiency, in [16], a bandwidth-efficient scheme for internally applying the error-correcting codes in fiber-optic CDMA systems has been proposed. It was shown that the internal-channel coding scheme significantly improves

Manuscript received May 2, 2006; revised December 17, 2006. This work was supported by the Iran National Science Foundation (INSF) under Contract 83173.

The authors are with the WRL, Electrical Engineering Department, Sharif University of Technology, Tehran 11365-9363, Iran (e-mail: fstabataba@ee.sharif.edu; s_aghajanzadeh@ee.sharif.edu; mnasiri@sharif.edu; karimi@ee.sharif.edu).

Color versions of one or more of the figures in this paper are available online at http://ieeexplore.ieee.org.

Digital Object Identifier 10.1109/JLT.2007.891173

the performance of the uncoded system without requiring any bandwidth expansion further than what is needed by the uncoded conventional OCDMA system. Recently, in [17], a new internally coded scheme for noncoherent TH-OCDMA system has been proposed, which is less complex than the method in [16]. Like in [16], a superorthogonal encoder is used in [17] as the internal code. However, in the method proposed in [17], in contrast to [16], the encoder outputs are considered as a sequence of symbols instead of bits.

In this paper, we apply the internally coded scheme, first introduced in [17], to the CULP CDMA system.[1] In this method, each bit's duration is divided into N_s frames. Two PN sequences are assigned to each user, named PN1 and PN2. In each bit interval, based on the PN1 sequence component and the channel encoder output, one of the N_s frames is selected, in which the spectral phase-coded pulse is transmitted. The PN2 sequence determines the phase mask pattern which is used to encode the phase of the ultrashort pulse in the spectral domain, i.e., the ultrashort pulse is multiplied by the PN sequence in the frequency domain. The encoded signal is broadened and becomes noiselike in the time domain. The decoder of the desired user compensates the phase offset simply by multiplying the received signal by the user's PN2 sequence in the spectral domain.

We consider two decoding techniques at the receiver, namely soft decoding and hard decoding. We evaluate the multiple access performance of these detection techniques in the presence of a thermal noise, using both the saddle point approximation and the Chernoff bound. We compare the results with those of the conventional CULP CDMA system. We show that the hard decoder has the best performance at a large number of users.

The rest of this paper is organized as follows: Section II describes our proposed system. In Section III, we analyze the performance of the system for the soft decoder with and without the thermal noise. In Section IV, we evaluate the performance of the hard decoder. In Section V, some numerical results are presented, and finally, in Section VI, this paper is concluded.

II. System Description

In this system, the bit duration, i.e., T_b, is divided into N_s frames. Let the duration of each frame be T_f, then we have $T_b = N_s T_f$. Two PN sequences, namely PN1 and PN2, are assigned to each user. The components of the PN1 and PN2 sequences are i.i.d. integer-valued random variables with a uniform distribution on $\{0, 1, \ldots, N_s - 1\}$ and $\{-1, 1\}$, respectively.

We assume that the uncoded ultrashort pulse has a flat spectrum with a bandwidth of W which is divided into N_0 chips; therefore, each chip has a bandwidth of $\Omega = W/N_0$. The spectrum of the uncoded ultrashort pulse is considered as follows:

$$A(\omega) = \left\{ \begin{array}{ll} \frac{\sqrt{P_0}}{W} & -\frac{W}{2} \le \omega \le \frac{W}{2} \\ 0 & \end{array} \right\} \tag{1}$$

where P_0 is the peak power of the ultrashort pulse.

[1]It should be noted that the internally coded scheme in [16] cannot be applied to the CULP CDMA systems.

The phase of each chip is adjusted independently by multiplying the uncoded pulse spectrum by a phase mask whose pattern is determined by the PN2 sequence components. A pseudorandom phase mask transforms the incident ultrashort pulse into a low-intensity pseudonoise burst. This pulse is transmitted in a frame which is determined by the output of the channel encoder and the PN1 sequence components at the corresponding bit interval. For the channel encoder, a superorthogonal convolutional code that is used as its path-generating function (which requires for the performance evaluation) is available.

Fig. 1(a) shows the block diagram of the transmitter. From this figure, the bit stream of each user n is applied to a superorthogonal convolutional encoder [19] with the constraint length K and rate $1/2^{K-2}$, which generates 2^{K-2} different symbols.[2] The encoder outputs are then added to the PN1 sequence in mod N_s, where $N_s = 2^{K-2}$. The result $(c_j^{(n)})$ specifies the position of one of the N_s frames. The phase-encoded ultrashort light pulse is then transmitted in the frame $c_j^{(n)}$

$$c_j^{(n)} = \left(s_j^{(n)} + \mathrm{PN1}_j^{(n)} \right) \bmod N_s \tag{2}$$

where $s_j^{(n)}$ and $\mathrm{PN1}_j^{(n)}$ are the encoder output and the PN1 sequence component of user n at jth bit interval, respectively. Let $E_i(t)$ be the spectral encoded pulse of the ith user, which can be written as [1]

$$E_i(t) = \frac{\sqrt{P_0}}{N_0} \sum_{m=-N}^{N} e^{-j\left(m\Omega t + \varphi_m^{(i)}\right)} \tag{3}$$

where $\varphi_m^{(i)} \in \{0, \pi\}$ denotes the mth code element of the ith user's transmitted signal. In the above equation, $N_0 = 2N + 1$ is the code length in the frequency domain [11]. Then, at the output of the star coupler during kth frame of jth bit interval, we have

$$s_k(t) = \sum_{i=1}^{u_k} E_i(t - jT_b + kT_f) \tag{4}$$

where u_k is the number of active users in the kth frame.

At the zeroth frame, in which the desired user sends its signal, we have

$$s_0(t) = E_n(t) + \underbrace{\sum_{i=1}^{u_0} E_i(t)}_{\mathrm{MAI}} \tag{5}$$

where $E_n(t)$ is the spectral encoded pulse of the desired user (user n), and $s_0(t)$ is the output of the star coupler during the zeroth frame.

[2]Note that in each bit interval, at the output of the channel encoder, we have a block of 2^{K-2} bits, which can only take 2^{K-2} different values. Each block can be represented by an integer number between 0 to 2^{K-2}, as a symbol. For details, see [19], as well as the structure of the encoder presented in Fig. 9.

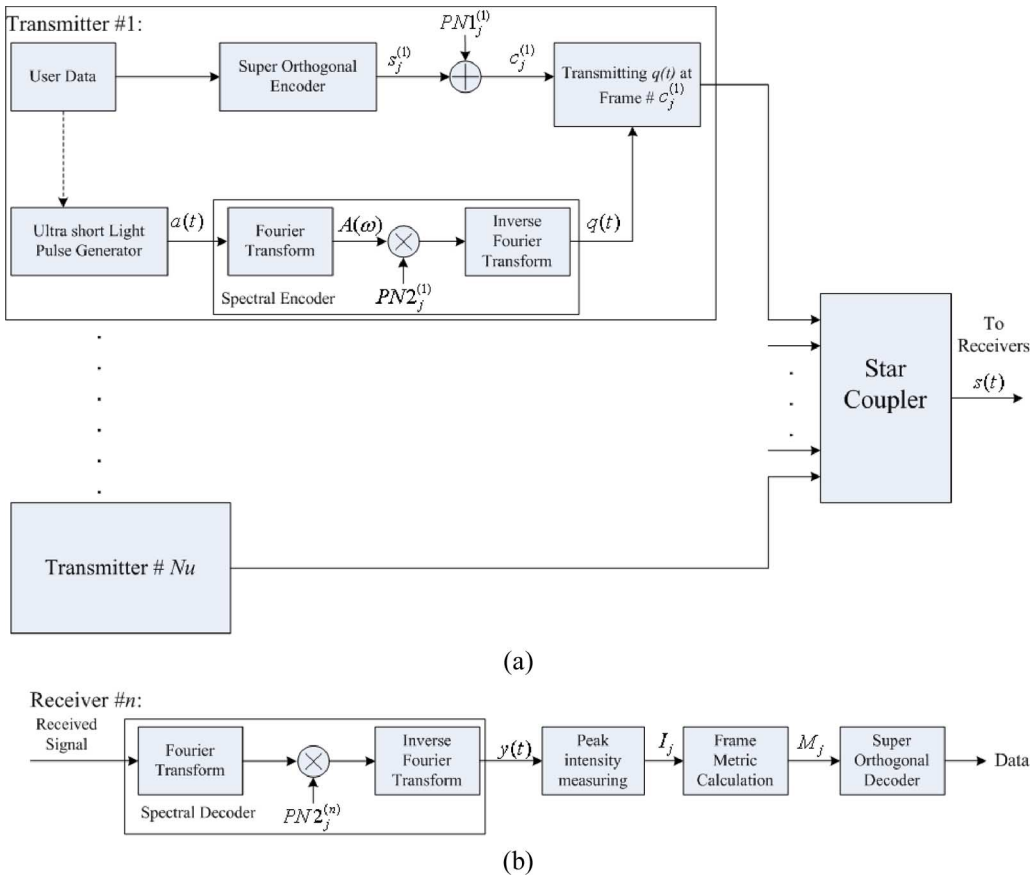

Fig. 1. Block diagram of the proposed system. (a) Structure of the transmitter. (b) Structure of the receiver for user n.

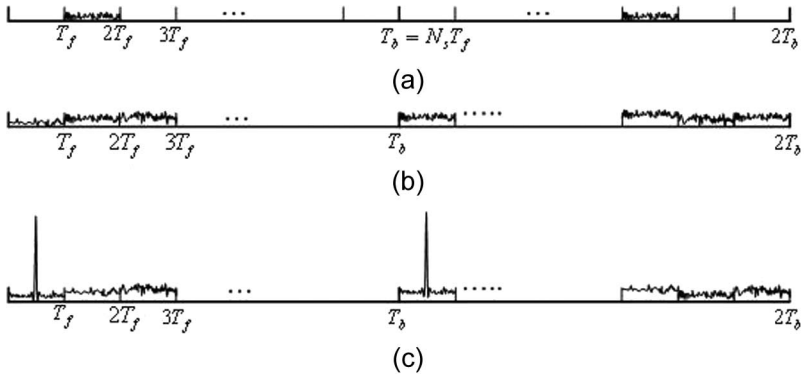

Fig. 2. Schematic timing diagram of the proposed system. (a) Typical transmitter signal. (b) Typical received signal at the input of the desired user's spectral decoder. (c) Signal at the output of the desired user's spectral decoder.

Fig. 1(b) shows the block diagram of the receiver for each user n. At the receiver front end, a typical spectral decoder is used which computes the correlation of the received signal with the desired signal by multiplying the received signal in the PN2 sequence of the desired user in the spectral domain. In fact, the nth optical decoder is similar to the nth optical encoder, except that the decoder's spectral-phase code is the complex conjugate of the encoder's spectral-phase code. Note that the spectral-phase code of each user depends only on the PN2 sequence. Fig. 2 demonstrates the schematic timing diagram of a typical transmitted signal and the received signal before and after the spectral decoder of the desired user. As can be realized from this figure, before the spectral decoder, the signals in all frames are noiselike, whereas after the spectral decoder, the phase shifts of the desired signal are removed, and the coherent ultrashort pulse of the user is reconstructed. However, for the undesired signals, the phase shifts are rearranged but not removed, and the signals at the output of the decoder remain as low-intensity pseudonoise burst.

At the output of the spectral decoder of the desired user during the kth frame, we have

$$y_k(t) = \sum_{i=1}^{u_k} E_{ni}(t) \tag{6}$$

where $E_{ni}(t)$ is the ith user signal $[E_i(t)]$ passing through the nth receiver. Therefore, for the zeroth frame, we have

$$y_0(t) = \underbrace{E_{nn}(t)}_{\text{Desired signal}} + \underbrace{\sum_{i=1, i\neq n}^{u_0} E_{ni}(t)}_{\text{MAI(noiselike signal)}} . \tag{7}$$

After the spectral decoder, there is an optical device that measures the peak intensity of the output in every frame time of each bit interval. Then, the underlying convolutional decoder uses these measurements for branch metric calculations of the related trellis diagram. The details will be explained in the following sections.

For performance evaluation, we assume that the first user is the desired user, which sends all-zero sequences. For the convolutional code, only the lower and upper bounds on the BER are analytically available which are computed using the path generating function of the code. For our application, as stated previously, the superorthogonal encoder outputs are considered as a sequence of symbols, in contrast with the scheme in [16], in which the encoder outputs are considered as a sequence of bits. There is a difference in using the outputs of the encoder as a sequence of bits or as a symbol. Consequently, the path generating function in our method differs from that in [19]. The path generating function in our application is computed as (see Appendix A)

$$T(D, N) = \frac{(1-D)ND^K}{1 - D\left(1 + N(1 + D^{K-3} - 2D^{K-2})\right)} \tag{8}$$

where in the series expansion of the above equation, the power of D denotes the (symbol) hamming weight of the encoder output, and the power of N represents the bit Hamming weight of the input. The number of bit errors due to an error event with weight d, i.e., a_d, can be calculated from the path generating function as follows [19]:

$$\left.\frac{\partial T(D, N)}{\partial N}\right|_{N=1} = \sum_{d=d_{\text{free}}}^{\infty} a_d D^d \tag{9}$$

where $d_f = k = \log_2 N_s + 2$ is the free distance of the code. Using a union bound, it can be easily shown that for the convolutional code, the upper bound on BER is as follows:

$$P_b < \sum_{d=d_{\text{free}}}^{\infty} a_d P_d \tag{10}$$

where P_d, which is an error event with a Hamming weight of d, is the probability that the metric of a nonzero path with the symbol weight d is larger than that of the all-zero path.

In the next sections, we evaluate P_d for the soft and hard decoding using the Chernoff bound and the saddle point approximation. Then, the BER is easily obtained using (10).

III. Soft Decoding Analysis

In this technique, after a typical spectral decoder in which the spectral-phase code is equal to the PN2 sequence of the desired user, an optical device is used to measure the peak intensity of the decoder's output in each frame time during each bit interval. Let $I_{j,k}$ be the peak intensity of the decoder's output during the kth frame of jth bit interval. Then, a metric value, i.e., $M_{j,k}$, is assigned to the frame (see Fig. 1). In the soft decoding technique, this metric is equal to the peak intensity. That is

$$M_{j,k} = I_{j,k}, \qquad k = 0, \ldots, N_s - 1. \tag{11}$$

The Viterbi decoder of the underlying convolutional code then utilizes these values to compute the branches' metrics of the Trellis diagram. That is, if the output symbol of a branch at the jth bit duration in the Trellis diagram is k, then the value $M_{j,k}$ is used as its metric.

As stated before, we assume that the first user is the desired user sending an all-zero data stream; therefore, the all-zero path is the one which is expected to have the largest metric. For BER evaluation [see (8)–(10)], we need to compute P_d. Considering the definition of P_d in (10), it can be easily shown that

$$\begin{aligned} P_d &= \Pr\left\{\sum_j M_{j,k} > \sum_j M_{j,0}\right\} \\ &= \Pr\left\{\sum_{i=1}^{d} M_{i,k\neq 0} > \sum_{i=1}^{d} M_{i,0}\right\} \\ &= \Pr\left\{\sum_{i=1}^{d} M_{i,k\neq 0} - \sum_{i=1}^{d} M_{i,0} > 0\right\} \\ &= \Pr\left\{\sum_{i=1}^{d} Z_i > 0\right\} \end{aligned} \tag{12}$$

where $Z_i = M_{i,k\neq 0} - M_{i,0}$ indicates the difference in the metrics of the branches corresponding to the nonzero and all-zero paths at instant of the ith different branches of the two paths. Note that the two paths may have a length larger than d, but they differ only in d branches.

We first compute the moment generating function (MGF) of Z_is. The variables Z_is are independent and have the same MGF. Therefore, we need to find the MGF of one of them. We have

$$Z_i = M_{i,k\neq 0} - M_{i,0}. \tag{13}$$

Note that because of the presence of the multiple access interference (MAI), the metrics of the branches corresponding to the nonzero and all-zero paths are not independent. Therefore, we compute the unconditional MGF using the MGF conditioned on the number of interfering users in each frame. Let u_k be the number of interfering users in frame k. Then, u_0 and u_k must satisfy $u_0 + u_k \leq N_u - 1$, where N_u is the total number of active users in the system, which makes the above two variables, i.e., $M_{i,0}$ and $M_{i,k}$ be dependent. However, conditioned on u_0 and u_k, these variables will be independent. Let $P(u_0, u_k)$ be the probability of having u_0 and u_k undesired

users in all-zero and nonzero frames (branches), respectively. We have

$$P(u_0,u_k)=\binom{N_u-1}{u_0}\binom{N_u-u_0-1}{u_k}\times\beta^{u_0+u_k}(1-2\beta)^{N_u-u_0-u_k-1} \quad (14)$$

where $\beta=1/N_s$ is the probability that a user sends its data in a specific frame. Then, we have

$$P(Z_i)=\sum_{u_0=0}^{N_u-1}\sum_{u_k=0}^{N_u-u_0-1}P(Z_i|u_0,u_k)P(u_0,u_k). \quad (15)$$

According to (14) and (15), we must compute $P(Z_i|u_0,u_k)$; therefore, from (11) and (13), we need to obtain the probability distribution functions (PDFs) of $I_{i,0}$ and $I_{i,k}$, i.e., the peak intensity of the spectral decoder's outputs during the first and kth frame. We know that the intensity of the signal is proportional to the square of its field magnitude. Field components of the signal in each frame time are well assumed to be jointly Gaussian random variables[3] [1]; therefore, the conditional PDFs of the signal peak intensity in the first and kth frame, i.e., $I_{i,0}$ and $I_{i,k}$, are

$$P_{I_{i,0}}(I)=\frac{N_0}{u_0P_0}e^{-\frac{I+P_0}{\frac{u_0P_0}{N_0}}}I_0\left(\frac{2N_0\sqrt{P_0\cdot I}}{u_0P_0}\right)$$
$$P_{I_{i,k}}(I)=\frac{N_0}{u_kP_0}e^{-\frac{N_0}{u_kP_0}I} \quad (16)$$

where N_0 is the code length of the PN2 sequence, and P_0 represents the peak power of an incident ultrashort pulse.[4] u_0 and u_k are defined in (14). $I_0(x)$ is the modified Bessel function of the first kind and zeroth order.

In order to find the MGF of Z_i, we need to obtain the MGFs of $I_{i,0}$ and $I_{i,k}$ which are derived as (see Appendix B)

$$\Phi_{I_{i,0}}(s)=\frac{1}{1-s\frac{u_0P_0}{N_0}}e^{\frac{sP_0}{1-s\frac{u_0P_0}{N_0}}}$$
$$\Phi_{I_{i,k}}(s)=\frac{1}{1-s\frac{u_kP_0}{N_0}} \quad (17)$$

where $I_{i,0}$ and $I_{i,k}$ are conditionally independent; therefore, from (11) and (13), we have

$$\Phi_{Z_i|u_0,u_k}(s)=\frac{1}{1-s\frac{u_kP_0}{N_0}}\cdot\frac{1}{1+s\frac{u_0P_0}{N_0}}\cdot e^{\frac{-sP_0}{1+s\frac{u_0P_0}{N_0}}}. \quad (18)$$

[3]Note that PN2 sequence is purely random code. Therefore, the field components due to the MAI are well modeled as Gaussian random variables.

[4]We assume that all users have the same power.

By taking the average on u_0 and u_k, we obtain

$$\begin{aligned}\Phi_{Z_i}(s)&=\sum_{u_0=0}^{N_u-1}\sum_{u_k=0}^{N_u-u_0-1}\Phi_{Z_i|u_0,u_k}(s)\cdot\binom{N_u-1}{u_0}\\&\quad\times\binom{N_u-u_0-1}{u_k}\beta^{u_0+u_k}(1-2\beta)^{N_u-u_0-u_k-1}\\&=\sum_{u_0=0}^{N_u-1}\sum_{u_k=0}^{N_u-u_0-1}\frac{1}{1-s\frac{u_kP_0}{N_0}}\cdot\frac{1}{1+s\frac{u_0P_0}{N_0}}\cdot e^{\frac{-sP_0}{1+s\frac{u_0P_0}{N_0}}}\\&\quad\times\binom{N_u-1}{u_0}\binom{N_u-u_0-1}{u_k}\cdot(1-2\beta)^{N_u-u_0-u_k-1}.\end{aligned} \quad (19)$$

In order to calculate P_d, we need the MGF of $Z=\sum_{i=1}^{d}Z_i$. Because of the independence of Z_is, we have

$$\Phi_Z(s)=\left(\Phi_{Z_i}(s)\right)^d. \quad (20)$$

The above derivations have been obtained in the absence of dark current and thermal noise. In the following, we consider the effect of the thermal noise. Note that since the integration time for an ultrashort pulse is very short, the effect of the dark current is commonly neglected. At the output of the optical device, the thermal Gaussian noise is added to the signal intensity. Therefore, the MGF of $I_{i,0}$ and $I_{i,k}$ must be multiplied by the MGF of the thermal noise, i.e., $\Phi_n(s)$, which is equal to

$$\Phi_n(s)=\exp\left(s^2\sigma_n^2/2\right) \quad (21)$$

where σ_n^2 is the variance of the thermal noise. Then, (17) and (21) result in

$$\begin{aligned}\Phi_{Z_i|u_0,u_k}(s)&=\frac{1}{1-s\frac{u_kP_0}{N_0}}\cdot\frac{1}{1+s\frac{u_0P_0}{N_0}}\\&\quad\cdot e^{\frac{-sP_0}{1+s\frac{u_0P_0}{N_0}}}\cdot e^{\frac{s^2\sigma_{\rm th}^2}{2}}\cdot e^{\frac{(-s)^2\sigma_{\rm th}^2}{2}}\\\Rightarrow\Phi_{Z_i}(s)&=\sum_{u_0=0}^{N_u-1}\sum_{u_k=0}^{N_u-u_0-1}\Phi_{Z_i|u_0,u_k}(s)\cdot\binom{N_u-1}{u_0}\\&\quad\times\binom{N_u-u_0-1}{u_k}\beta^{u_0+u_k}(1-2\beta)^{N_u-u_0-u_k-1}\\&=e^{s^2\sigma_{\rm th}^2}\\&\quad\cdot\left[\sum_{u_0=0}^{N_u-1}\sum_{u_k=0}^{N_u-u_0-1}\frac{1}{1-s\frac{u_kP_0}{N_0}}\cdot\frac{1}{1+s\frac{u_0P_0}{N_0}}\right.\\&\quad\cdot e^{\frac{-sP_0}{1+s\frac{u_0P_0}{N_0}}}\binom{N_u-1}{u_0}\binom{N_u-u_0-1}{u_k}\\&\quad\left.\cdot(1-2\beta)^{N_u-u_0-u_k-1}\beta^{u_0+u_k}\right].\end{aligned} \quad (22)$$

By substituting (22) in (20), the MGF $\Phi_Z(s)$ is calculated. Then, the P_d in (12) and, as a result, the BER of the system, i.e., P_b, can be derived using the Chernoff bound or saddle point approximation, as follows.

For the Chernoff bound, we have

$$P_d = P(Z > 0) \le \Phi_Z(s_0) = \min_s \Phi_Z(s) \tag{23}$$

where s_0 is the value of s in which the MGF has its minimum value. We obtain the minimum of $\Phi_Z(s)$ by numerical calculation.

For the saddle point approximation, we must calculate the minimum of $\psi(s)$ (See Appendix C):

$$\psi(s) = -\ln(s) + \ln\left(\Phi_Z(s)\right) = -\ln s + d\ln\left(\Phi_{Z_i}(s)\right) \tag{24}$$

where $\Phi_{Z_i}(s)$ is as defined in (22). Then, we have

$$P_d \approx \frac{\exp\left(\psi(s_0)\right)}{\sqrt{2\pi\psi''(s_0)}} \tag{25}$$

where s_0 is the minimum point of $\psi(s)$ that is calculated numerically.

IV. Hard Decoding

In this receiver, a threshold device is used after the spectral decoder that compares the peak intensity of the decoder's output in each frame k during each bit interval i, i.e., $I_{i,k}$, with the threshold $I_{\rm th}$. If the peak intensity of decoder's output is higher than the threshold level, the metric assigned to the frame is 1, i.e., $M_{i,k} = 1$; otherwise, it is zero:

$$M_{i,k} = \begin{cases} 1, & \text{if } I_{i,k} > I_{\rm th} \\ 0, & \text{if } I_{i,k} < I_{\rm th}. \end{cases} \tag{26}$$

Like in the soft decoding, these values are then used for branch metric calculations of the Trellis diagram of the underlying convolutional codes (see Section III for more details). Considering the definition of P_d in (10), which is the same as for the soft decoding [see (12)], we have

$$P_d = \Pr\left\{ Z = \sum_{i=1}^{d} Z_i > 0 \right\} \tag{27}$$

where $Z_i = M_{i,k\neq 0} - M_{i,0}$ takes on values 0, -1, and 1 for the hard decoder, and its MGF is obtained as follows:

$$\begin{aligned} \Phi_{Z_i}(s) &= E(e^{Z_i s}) \\ &= P(1)e^{s} + P(0) + P(-1)e^{-s} \\ \Rightarrow \Phi_Z(s) &= \left(\Phi_{Z_i}(s)\right)^d \\ &= \left(P(1)e^{s} + P(0) + P(-1)e^{-s}\right)^d \end{aligned} \tag{28}$$

where $P(0)$, $P(1)$, or $P(-1)$ is the probability that Z_i equals to 0, 1, or -1, respectively. In order to find these probabilities, we use the conditional probability as follows:

$$P(1) = P(Z_i = 1) = \sum_{u_0=0}^{N_u-1} \sum_{u_k=0}^{N_u-u_0-1} P(Z_i = 1|u_0, u_k) P(u_0, u_k) \tag{29}$$

where $P(u_0, u_k)$ is as defined in (14). Because $M_{i,0}$ and $M_{i,k}$ (when conditioned on u_0 and u_k) are independent, we have

$$P(Z_i = 1|u_0, u_k) = P(M_{i,k} = 1|u_0, u_k) P(M_{i,0} = 0|u_0, u_k). \tag{30}$$

From (16) and (26), these probabilities can be easily calculated as [1]

$$\begin{aligned} P(M_{i,k} = 1|u_0, u_k) &= P(I_{i,k} > I_{\rm th}|u_0, u_k) \\ &= \int_{I_{\rm th}}^{\infty} \frac{N_0}{u_k P_0} e^{-\frac{I N_0}{u_k P_0}} dI = e^{-\frac{I_{\rm th} N_0}{u_k P_0}} \\ P(M_{i,0} = 0|u_0, u_k) &= P(I_{i,0} < I_{\rm th}|u_0, u_k) \\ &= \int_{0}^{I_{\rm th}} \frac{N_0}{u_0 P_0} e^{-\frac{I + P_0}{\frac{u_0 P_0}{N_0}}} I_0\left(\frac{2N_0\sqrt{P_0 I}}{u_0 P_0}\right) dI \\ &= 1 - Q\left(\sqrt{\frac{2N_0}{u_0}}, \sqrt{\frac{2N_0 I_{\rm th}}{u_0 P_0}}\right) \end{aligned} \tag{31}$$

where $Q(a,b) = \int_b^\infty x \exp((-a^2 - x^2)/2) I_0(ax) dx$. From (29)–(31), we obtain

$$\begin{aligned} P(1) &= \sum_{u_0=0}^{N_u-1} \sum_{u_k=0}^{N_u-u_0-1} P(M_{i,k} = 1|u_0, u_k) \\ &\quad \cdot P(M_{i,0} = 0|u_0, u_k) P(u_0, u_k) \\ &= \sum_{u_0=0}^{N_u-1} \sum_{u_k=0}^{N_u-u_0-1} e^{-\frac{I_{\rm th} N_0}{u_k P_0}} \\ &\quad \cdot \left(1 - Q\left(\sqrt{\frac{2N_0}{u_0}}, \sqrt{\frac{2N_0 I_{\rm th}}{u_0 P_0}}\right)\right) P(u_0, u_k). \end{aligned} \tag{32}$$

Similarly, for $P(-1)$ and $P(0)$, we have

$$\begin{aligned} P(-1) &= P(Z_i = -1) \\ &= \sum_{u_0=0}^{N_u-1} \sum_{u_k=0}^{N_u-u_0-1} P(M_{i,k} = 0|u_0, u_k) \\ &\quad \times P(M_{i,0} = 1|u_0, u_k) P(u_0, u_k) \\ &= \sum_{u_0=0}^{N_u-1} \sum_{u_k=0}^{N_u-u_0-1} \left(1 - e^{-\frac{I_{\rm th} N_0}{u_k P_0}}\right) \\ &\quad \cdot Q\left(\sqrt{\frac{2N_0}{u_0}}, \sqrt{\frac{2N_0 I_{\rm th}}{u_0 P_0}}\right) P(u_0, u_k) \end{aligned} \tag{33}$$

$$P(0) = \sum_{u_0=0}^{N_u-1} \sum_{u_k=0}^{N_u-u_0-1} [P(M_{i,k}=0|u_0,u_k)P(M_{i,0}=0|u_0,u_k) + P(M_{i,k}=1|u_0,u_k)P(M_{i,0}=1|u_0,u_k)] \times P(u_0,u_k)$$

$$= \sum_{u_0=0}^{N_u-1} \sum_{u_k=0}^{N_u-u_0-1} \left[\left(1-e^{-\frac{I_{\rm th}N_0}{u_kP_0}}\right)\cdot\left(1-Q\left(\sqrt{\frac{2N_0}{u_0}},\sqrt{\frac{2N_0I_{\rm th}}{u_0P_0}}\right)\right) + e^{-\frac{I_{\rm th}N_0}{u_kP_0}} Q\left(\sqrt{\frac{2N_0}{u_0}},\sqrt{\frac{2N_0I_{\rm th}}{u_0P_0}}\right)\right] P(u_0,u_k). \quad (34)$$

By substituting (32)–(34) in (28), the MGF of Z_i and, as a result, the MGF of Z [from (20)] are computed. From (10) and (27), the BER is calculated from $\Phi_Z(s)$ using the Chernoff bound and saddle point approximation, as follows.

For the Chernoff bound, we must find the minimum of $\Phi_Z(s)$:

$$\frac{\partial\Phi_Z(s)}{\partial s} = 0 \Rightarrow d\left(P(1)e^s - P(-1)e^{-s}\right) \times \left(P(1)e^s + P(0) + P(-1)e^{-s}\right)^{d-1} = 0$$

$$\Rightarrow s_0 = \frac{1}{2}\ln\left(\frac{P(-1)}{P(1)}\right). \quad (35)$$

Then, from (12) and (23), we have

$$P_d \le \Phi_Z(s_0) = \left(P(0) + 2\sqrt{P(1)P(-1)}\right)^d. \quad (36)$$

For the saddle point approximation, we must calculate the minimum of $\psi(s)$:

$$\psi(s) = -\ln(s) + \ln\left(\Phi_Z(s)\right)$$

$$= -\ln s + d\ln\left(P(1)e^s + P(0) + P(-1)e^{-s}\right)$$

$$\Rightarrow \psi'(s) = -\frac{1}{s} + d\frac{P(1)e^s - P(-1)e^{-s}}{P(1)e^s + P(0) + P(-1)e^{-s}} = 0$$

$$\Rightarrow P(1)e^s(ds-1) - P(-1)e^{-s}(ds+1) - P(0) = 0. \quad (37)$$

The root of the last equation in (37) is computed numerically and substituted in (C3) to obtain P_d.

When considering the thermal noise effect, we take exactly the same steps as above, only $P(0)$, $P(1)$, and $P(-1)$ must be recomputed using the MGFs of $I_{i,0}$, $I_{i,k}$, and the thermal noise. Therefore, according to (17) and (21), we have

$$\Phi_{I_{i,0}}(s) = \frac{1}{1-s\frac{u_0P_0}{N_0}} e^{\frac{sP_0}{1-s\frac{u_0P_0}{N_0}}} \cdot e^{\frac{s^2\sigma_n^2}{2}}$$

$$\Phi_{I_{i,k}}(s) = \frac{1}{1-s\frac{u_kP_0}{N_0}} \cdot e^{\frac{s^2\sigma_n^2}{2}}. \quad (38)$$

Then, from (38), these probabilities [$P(0)$, $P(1)$, and $P(-1)$] can be easily computed using the saddle point approximation or a Beaulieu series [20]. Note that for high-value probabilities, the Beaulieu series is more accurate. However, for the error rates less than 10^{-8}, the Beaulieu series is not valid, and the saddle point approximation is used. Therefore, we have utilized the Beaulieu series and the saddle point approximation for computing $P(I_{i,0} > I_{\rm th}|u_0,u_k)$ and $P(I_{i,k} > I_{\rm th}|u_0,u_k)$, respectively.

V. Numerical Results

In this section, we evaluate the performance of the proposed multiple access scheme using analytical results obtained in the previous sections and compare the results with those of the conventional CULP CDMA. In all of the numerical results evaluated, we have used the superorthogonal code with rate 1/4; therefore, the constraint length of the code is $K = 4$, and N_s (the number of frames per bit) is 4. The path-generating function of the code is given in (8). Consider the following Taylor series expansion of the derivative of the function with $K = 4$:

$$\left.\frac{\partial T(D,N)}{\partial N}\right|_{N=1} = \sum_{d=d_{\rm free}}^{\infty} a_d D^d = D^4 + 2D^5 + 7D^6 + 16D^7 + 41D^8 + 94D^9 + \cdots. \quad (39)$$

Then, the BER can be obtained from (10) by substituting the coefficients a_ds from (39) in (10). Since P_d, which is the probability of an error event with the Hamming weight of d, decreases rapidly with d, for our numerical evaluations, we have well considered only the first ten terms. As previously stated, we use the Chernoff bound and the saddle point approximation to obtain the upper bound of BER from the MGFs.

Fig. 3 shows the plots of the BER of our proposed method (using Chernoff bound) and the conventional CULP CDMA versus the number of users for the soft decoder. In this figure, the effect of the thermal noise is not considered, and as in the conventional CULP CDMA system analyzed in [1], the effect of the thermal noise was neglected.

In order to have a fair comparison, the two schemes must have the same bandwidth or equivalently, the same processing gain (PG) of N_sN_0. That is, the spectral code length for the CULP CDMA (uncoded scheme) is N_s times that of our proposed scheme. In addition, we assume the best case for the uncoded system, i.e., we suppose that the optical pulse in the CULP CDMA system is transmitted in whole bit time ($T_b = KT$, where $K = 1$) [1], [18]. Therefore, in the BER

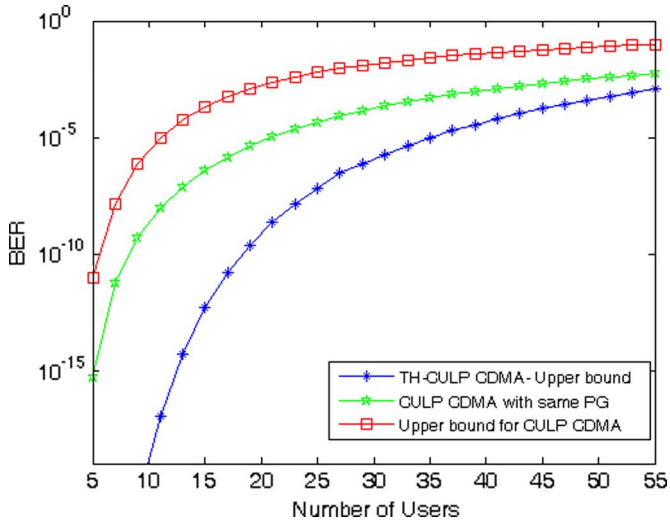

Fig. 3. Plots of BER for the proposed scheme (Chernoff Bound) using the soft decoder and for the conventional CULP CDMA (including both exact BER and the upper bound) with the same PG, $N_0 = 127$ (Code length in frequency domain), and $N_s = 4$ (number of frames).

equation derived in [1], we need to substitute N_0 by $N_s N_0$, $K = 1$, $I_{\text{th}} = P_0/4$.

In Fig. 3, we have also included the plot of the upper bound on the BER of the CULP CDMA system taken from [18] as[5]

$$\begin{aligned} P_e &\le \sum_{l=1}^{N_u} P(l) e^{-\frac{\text{PG}}{4Kl}} \\ &\le e^{-\frac{\text{PG}}{4KN_u}} \sum_{l=1}^{N_u} P(l) \\ &\le e^{-\frac{\text{PG}}{4KN_u}}, \qquad \text{PG} = N_0 N_s \text{ and } K = 1 \\ \Rightarrow P_e &\le e^{-\frac{N_0 N_s}{4N_u}}. \end{aligned} \tag{40}$$

As can be realized from Fig. 3, our proposed scheme substantially outperforms the conventional CULP CDMA scheme. For instance, at BER of around 10^{-10}, the number of users supported by our method is about 18, while for the CULP CDMA, it is 7.

Fig. 4 shows the performance of our proposed scheme using the saddle point approximation for the soft decoder. The results for the conventional scheme are also included. It can be seen that the difference between the Chernoff bound and the saddle point approximation is not more than one or two orders of magnitude. As can be realized, our scheme works much better than the conventional method. At BER around 10^{-4}, the number of users supported by the CULP CDMA is less than 30, whereas for our proposed method, it is over 55. Note that in our method, the plots indicate the upper bound of the BER, while for the conventional CULP CDMA, they show the exact BER.

[5]Note that in our proposed scheme, the plots of P_b in fact indicate the upper bound of the bit error rate, whereas in the conventional CULP CDMA, the plots show the exact bit error probability.

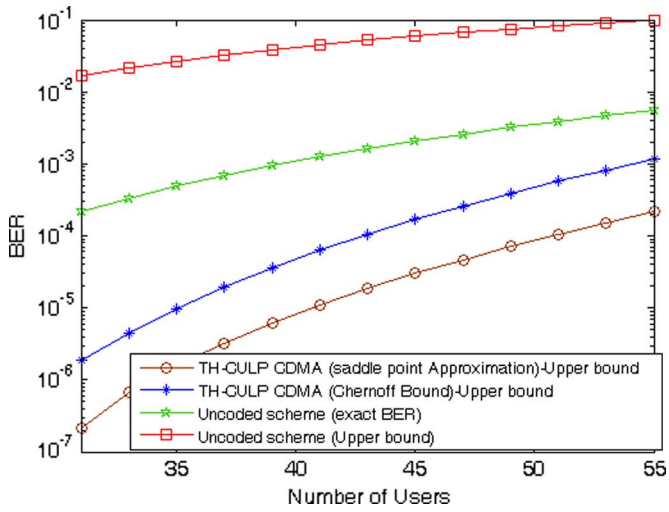

Fig. 4. Plots of BER versus the number of users for the soft decoder, $N_0 = 127$, and $N_s = 4$.

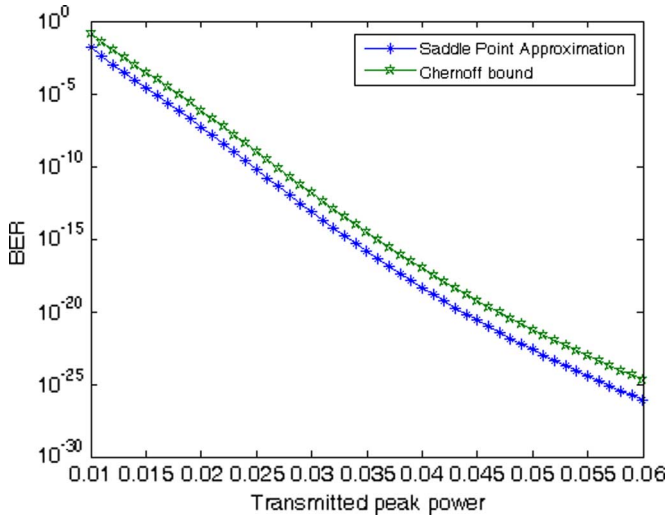

Fig. 5. Plots of the BER of the proposed scheme versus the transmitted peak power, for soft decoder considering the effect of the thermal noise on the performance, $N_u = 5$, $N_0 = 127$, $N_s = 4$, and $\sigma_n = 5\text{e} - 3$.

In Fig. 5, the effect of the thermal noise has been considered on the performance of the soft decoder. This figure demonstrates the performance of the system versus the transmitted peak power considering the thermal noise effect.

As stated previously, in the hard decoding, the BER depends on the normalized threshold (I_{th}/P_0), and it must be selected properly. Fig. 6 shows the plots of BER for the hard decoder versus the normalized threshold for various numbers of users. As can be realized, the optimum threshold value depends on the number of users. The optimum threshold value also depends on the system's PG.[6]

In Fig. 7, the performance of the hard and soft decoders has been compared. As could be well expected, the hard decoder outperforms the soft decoder when there are a high number of users. The reason is that, when there are a large number of users, the MAI results in a high intensity value in incorrect

[6]Increasing the PG of the system results in the reduction of the interference intensity, which leads to the decrement of the optimum threshold value.

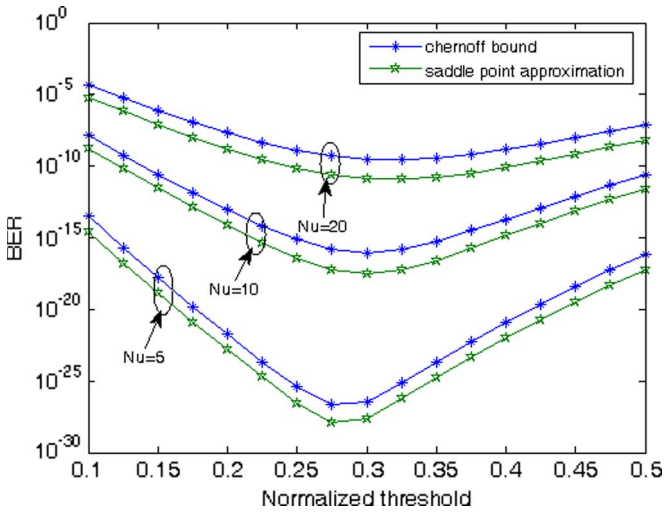

Fig. 6. Plots of BER versus normalized threshold for 5, 10, and 20 users, for hard decoder, $N_0 = 127$, and $N_s = 4$.

frames (nonzero frames), whereas the hard decoder suppresses this value to 1 and hereby reduces substantially its destructive effects, but it does not necessarily hold when there are a low number of users.[7]

In Fig. 8, the plots of BER for the hard decoder for various values of the thermal noise variance have been presented. As can be realized, the effect of the thermal noise is less for the large number of users because, when there are a high number of users, the devastating effect of the MAI is more substantial than the thermal noise.

VI. Conclusion

In this paper, a new internally coded TH CULP CDMA system has been considered which does not require any extra bandwidth compared to what is required by the uncoded system. We have considered the effects of the MAI and the thermal noise on the performance of the system for both soft and hard decoders. The probability of error has been evaluated using the Chernoff bound and the saddle point approximation. We have compared our proposed system with the conventional CULP CDMA system. The numerical results have indicated that our proposed system performs substantially better than the conventional CULP CDMA system at the same bit rate and PG. In addition, it has been shown that the hard decoder has the best performance when there are large number of users, whereas the soft decoder has better results when there are a small number of users.

[7]Note that the multiple access scheme proposed (TH-CULP CDMA) is a combination of the interference averaging (CULP CDMA) and the interference avoiding (TH-CDMA) techniques. For a pure interference avoiding technique (like optical orthogonal CDMA and TH-CDMA), the chip-level hard limiter decoder always works better than the soft decoder, regardless of the number of users when considering only the MAI as a noise. On the other hand, for a pure interference averaging technique (like CULP CDMA or DS-CDMA), the soft decoder always performs better than the hard decoder. Therefore, when there are a small number of users in which the intensity level is not so high at the incorrect frames (nonzero frames) to frequently exceed the threshold, the interference averaging technique is more efficient to reduce the interference, and as a result, the soft-input decoder can perform better than the hard-input decoder.

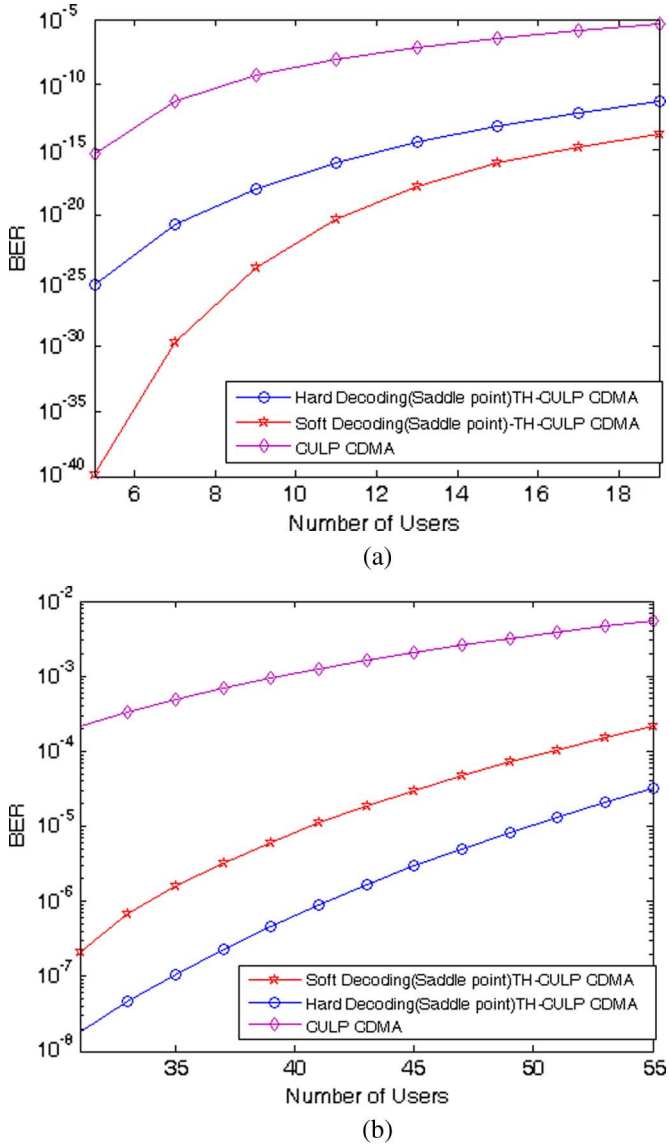

Fig. 7. Plots of the BER of the proposed scheme for different decoding methods in comparison with conventional CULP CDMA scheme, $N_0 = 127$, and $N_s = 4$. (a) Small number of users. (b) Large number of users.

Appendix A
Derivation of the Path Generating Function of the Super Orthogonal Codes [21]

Fig. 9 shows the block diagram of the superorthogonal encoder considered in this paper. The $K-2$ bits (the contents of the first $K-2$ stages) of the $(K-1)$-stage shift register of the encoder are added to the first (input) and last (output) bits, and then, the outputs are applied to a Walsh–Hadamard orthogonal encoder [23] to generate one of the 2^{K-2} possible symbols. Note that the output of the Walsh–Hadamard encoder is zero only when all its $K-2$ input bits are zero.

In order to find the path generating function of the code, we apply the method introduced by Einarsson *et al.* [22]. This method uses a simplified state diagram shown in Fig. 10. In this diagram, "N" and "D" indicate the bit weight of the input and the symbol weight of the output, respectively. In other words, a gain N in a branch shows that the corresponding input

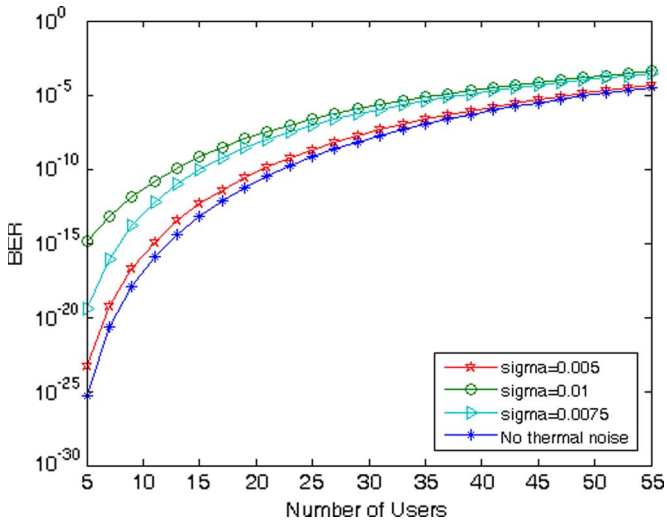

Fig. 8. Plots of BER versus the number of users for various values of σ_n, using hard decoder, $N_0 = 127$, and $N_s = 4$.

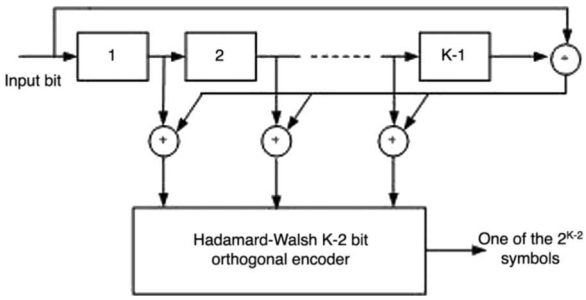

Fig. 9. Block diagram of the superorthogonal encoder used in this paper.

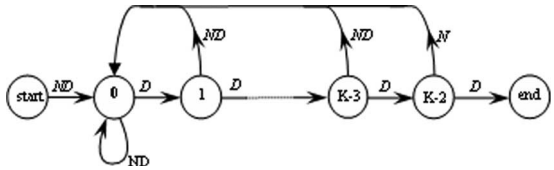

Fig. 10. Simplified state diagram of the encoder.

is "1," and a gain D implies that the corresponding output is a nonzero symbol. In Fig. 10, a state is defined as the number of consecutive zero bits in the left side of the shift register. The diagram begins at the "start" state and ends at the "end" state. An input bit "1" leads to going from the "start" state to the "zero" state. Then, by each "0" input bit, we move one state toward the state diagram and, by each bit of "1" entering the shift register, we return back to the "zero" state. In all these cases, except for the state $K-2$, the output symbol will be nonzero, which is depicted in the state diagram by a gain factor "D." Note that for the last stage, for an input bit "1," the output symbol is zero, which is denoted in the state diagram by a gain factor of $D^0 = 1$. The "end" state happens when the $(K-1)$ th "0" bit enters the shift register, and we return to the all-zero state. Note that before entering the "end" state, the last "1" bit in the shift register negates all the input bits to the Walsh–Hadamard encoder that results in a nonzero output symbol.

Having completed the state diagram, the path generating function can be easily found using the Mason rule to calculate the transfer function from the "start" state to the "end" state. It is obtained as

$$\begin{aligned} T(D,N) &= \frac{\text{Forward Path}}{1-\text{Loops}} \\ &= \frac{ND\cdot D^{k-2}\cdot D}{1-N(D+D^2+D^3+\cdots+D^{k-2}+D^{k-2})} \\ &= \frac{N\cdot D^K}{1-N\left(D\frac{1-D^{k-2}}{1-D}+D^{k-2}\right)} \\ &= \frac{(1-D)ND^k}{1-D\left(1+N(1+D^{k-3}-2D^{k-2})\right)} \end{aligned} \tag{A1}$$

which was used in (8).

Appendix B
MGFs of the Negative Exponential and Noncentral Chi-Square Random Variables

In this Appendix, we calculate the MGFs of two random variables $I_{i,0}$, $I_{i,k}$ defined in (16). Suppose that r denotes the peak of the signal at the spectral decoder output. The real and imaginary parts of r are modeled as jointly Gaussian random variables [1]; therefore, we have

$$r = r_x + jr_y, \quad r_x \sim N(\mu_x,\sigma^2), \quad r_y \sim N(\mu_y,\sigma^2). \tag{B1}$$

Then, we obtain

$$\begin{aligned} \Phi_{|r|^2}(s) &= E(e^{sI}) \\ &= E(e^{s|r^2|}) \\ &= E\left(e^{s(r_x^2+r_y^2)}\right) \\ &= E(e^{sr_x^2})E(e^{sr_y^2}) \\ &= \left[\frac{1}{\sqrt{2\pi\sigma^2}}\int_{-\infty}^{+\infty} e^{-\frac{1}{2}\frac{(r_x-\mu_x)^2}{\sigma^2}+sr_x^2}dr_x\right] \\ &\quad\times\left[\frac{1}{\sqrt{2\pi\sigma^2}}\int_{-\infty}^{+\infty} e^{-\frac{1}{2}\frac{(r_y-\mu_y)^2}{\sigma^2}+sr_y^2}dr_y\right] \end{aligned} \tag{B2}$$

$$\begin{aligned} \Phi_{|r|^2}(s) &= \frac{1}{\sqrt{1-2s\sigma^2}}e^{\frac{\mu_x^2 s}{\sqrt{1-2s\sigma^2}}}\cdot\frac{1}{\sqrt{1-2s\sigma^2}}e^{\frac{\mu_y^2 s}{\sqrt{1-2s\sigma^2}}} \\ &= \frac{1}{1-2s\sigma^2}e^{\frac{(\mu_x^2+\mu_y^2)s}{1-2s\sigma^2}} \quad \text{if } s<\frac{1}{2\sigma^2}. \end{aligned} \tag{B3}$$

Note that the above MGF is valid for the value of s less than $1/2\sigma^2$. Let u_0 and u_k be as defined in (19). Then, for variable $I_{i,0} = |r|^2$ and $I_{i,k}$, we, respectively, obtain $\sigma^2 = (u_0P_0)/(2N_0)$ and $\sigma^2 = (u_kP_0)/(2N_0)$ [1]. Also, for the nonzero path, the mean of both Gaussian variables (r_x, r_y) is zero, but for all-zero path, $\mu_x = \sqrt{P_0}$, $\mu_y = 0$; therefore, (B2) yields

$$\begin{aligned} \Phi_{I_{i,0}}(s) &= \frac{1}{1-s\frac{u_0P_0}{N_0}}e^{\frac{sP_0}{1-s\frac{u_0P_0}{N_0}}} \\ \Phi_{I_{i,k}}(s) &= \frac{1}{1-s\frac{u_kP_0}{N_0}}. \end{aligned} \tag{B4}$$

Note that from (B2), variable "s" should be smaller than $1/2\sigma^2$. Since the maximum value for u_0 or u_k is (N_u-1), we obtain

$$\sigma^2_{\max} = \frac{(N_u-1)P_0}{2N_0}. \tag{B5}$$

Therefore, from the above restriction for s, we obtain

$$s < \frac{N_0}{(N_u-1)P_0}. \tag{B6}$$

APPENDIX C
SADDLE POINT APPROXIMATION [22]

In this Appendix, we introduce the saddle point approximation to compute the probability from the MGF. Let $p(x)$ and $\Phi_X(s)$ be the pdf and MGF of a random variable X. Also, let us define

$$q_+(\alpha) = \int_{\alpha}^{\infty} p(x)dx = P(X > \alpha) \tag{C1}$$

$$q_-(\alpha) = \int_{-\infty}^{\alpha} p(x)dx = P(X < \alpha). \tag{C2}$$

For the saddle point approximation, we have

$$q_+(\alpha) \approx \frac{\exp\left(\psi(s_0)\right)}{\sqrt{2\pi\psi''(s_0)}} \tag{C3}$$

$$q_-(\alpha) \approx \frac{\exp\left(\psi(s_1)\right)}{\sqrt{2\pi\psi''(s_1)}} \tag{C4}$$

where

$$\exp\left(\psi(s)\right) = |s|^{-1}\exp(-s\alpha)\Phi_X(s) \tag{C5}$$

where s_0 and s_1 are the positive and negative roots of $\psi'(s)=0$, respectively. Note that for solving $\psi'(s)=0$, the Newton–Raphson method can be used.

REFERENCES

[1] J. A. Salehi, A. M. Weiner, and J. P. Heritage, "Coherent ultrashort light pulse code-division multiple access communication systems," *J. Lightw. Technol.*, vol. 8, no. 3, pp. 478–491, Mar. 1990.

[2] H. P. Sardesai, C.-C. Chang, and A. M. Weiner, "A femtosecond code-division multiple-access communication system test bed," *J. Lightw. Technol.*, vol. 16, no. 11, pp. 1953–1964, Nov. 1998.

[3] W. Naoya and K. I. Kitayama, "A 10 Gb/s optical code division multiplexing using 8-chip optical bipolar code and coherent detection," *J. Lightw. Technol.*, vol. 17, no. 10, pp. 1758–1765, Oct. 1999.

[4] K. Kamakurat, Y. Gamachit, H. Ueharat, and I. Sasaset, "Optical CDMA based on frequency-domain encoding enhancement of frequency division multiplexing," in *Proc. IEEE Pacific Rim Conf. Commun., Comput. and Signal Process. "10 Years PACRIM 1987–1997—Networking the Pacific Rim,"* 1997, pp. 611–614.

[5] D. Zaccarin and M. Kavehrad, "Performance evaluation of optical CDMA systems using noncoherent detection and bipolar codes," *J. Lightw. Technol.*, vol. 12, no. 1, pp. 96–105, Jan. 1994.

[6] M. Kavehrad and D. Zaccarin, "Optical code-division-multiplexed systems based on spectral encoding of noncoherent sources," *J. Lightw. Technol*, vol. 13, no. 3, pp. 534–545, Mar. 1995.

[7] X. Wang, N. Wada, T. Hamanaka, K.-I. Kitayama, and A. Nishiki, "10-user, truly-asynchronous OCDMA experiment with 511-chip SSFBG en/decoder and SC-based optical thresholder," presented at the Conf. Optical Fiber Commun. (OFC), Los Angeles, CA, Mar. 2005, Paper PDP33.

[8] Z. Jiang, D. S. Seo, S.-D. Yang, D. E. Leaird, R. V. Roussev, C. Langrock, M. M. Fejer, and A. M. Weiner, "Four-user, 2.5-Gb/s, spectrally coded OCDMA system demonstration using low-power nonlinear processing," *J. Lightw. Technol.*, vol. 23, no. 1, pp. 143–158, Jan. 2005.

[9] X. Wang, K. Matsushima, A. Nishiki, N. Wada, F. Kubota, and K.-I. Kitayama, "Experimental demonstration of 511-chip 640 Gchip/s superstructured FBG for high performance optical code processing," presented at the 30th Eur. Conf. Optical Commun. (ECOC), Stockholm, Sweden, Sep. 2004, Paper Tu 1.3.7.

[10] R. Papannareddy and A. M. Weiner, "Performance Comparison of coherent ultrashort light pulse and incoherent broadband CDMA systems," *IEEE Photon. Technol. Lett.*, vol. 11, no. 12, pp. 1683–1685, Dec. 1999.

[11] J. Y. Kim and H. V. Poor, "Turbo-coded packet transmission for an optical CDMA network," *J. Lightw. Technol.*, vol. 18, no. 12, pp. 1905–1916, Dec. 2000.

[12] R. Gold, "Optimal binary sequences for spread spectrum multiplexing," *IEEE Trans. Inf. Theory*, vol. IT-13, no. 4, pp. 619–621, Oct. 1967.

[13] M. R. Dale and R. M. Gagliardi, "Channel coding for asynchronous fiber-optic CDMA communications," *IEEE Trans. Commun.*, vol. 43, no. 9, pp. 2485–2492, Sep. 1995.

[14] J. Y. Kim and H. V. Poor, "Turbo-coded packet transmission for an optical CDMA network," *J. Lightw. Technol.*, vol. 18, no. 12, pp. 1905–1916, Dec. 2000.

[15] H. Pasqual and H. Yashima, "Analysis of optical PPM/CDMA system with M-ary convolutional coding," *IEICE Trans. Commun.*, vol. E82-B, no. 10, pp. 1618–1625, Oct. 1999.

[16] P. Azmi, M. Nasiri-Kenari, and J. A. Salehi, "Low-rate super orthogonal channel coding for fiber-optic CDMA communication systems," *J. Lightw. Technol.*, vol. 19, no. 6, pp. 847–855, Jun. 2001.

[17] M. Karimi and M. Nasiri Kenari, "An internally coded TH/OCDMA scheme for fiber optic communication systems and its performance analysis Part I: Using optical orthogonal code," *IEEE Trans. Commun.*, Feb. 2007. to be published.

[18] D. J. Hajela and J. A. Salehi, "Limits to the encoding and bounds on the performance of coherent ultrashort light pulse code-division multiple-access systems," *IEEE Trans. Commun.*, vol. 40, no. 2, pp. 325–336, Feb. 1992.

[19] A. J. Viterbi, *CDMA: Principles of Spread Spectrum Communications*. Reading, MA: Addison-Wesley, 1995.

[20] N. C. Beaulieu, "An infinite series for the computation of the complementary probability distribution function of *s* sum of independent random variables and its application to the sum of Rayleigh random variables," *IEEE Trans. Commun.*, vol. 38, no. 9, pp. 1463–1474, Sep. 1990.

[21] Y. Motadayen Aval, "A new coding method in MC-FH-CDMA systems," M.S. thesis, Sharif Univ. Tech., Tehran, Iran, Jan. 2005.

[22] G. Einarsson, *Principles of Lightwave Communications*. New York: Wiley, 1996.

[23] S. B. Wicker, *Error Control Systems for Digital Communication and Storage*. Englewood Cliffs, NJ: Prentice-Hall, 1995.

Foroogh S. Tabataba was born in 1982. She received the B.S. degree (with honors) from Isfahan University of Technology, Isfahan, Iran, in 2004 and the M.S. degree from Sharif University of Technology, Tehran, Iran, in 2006, both in electrical engineering. She is currently working toward the Ph.D. degree with the Department of Electrical Engineering, Sharif University of Technology.

Since March 2004, she has been a Research Assistant with the Advanced Communication Research Institute, Wireless Research Laboratory of the Electrical Engineering Department, Sharif University of Technology. Her research interests include optical communication systems, specifically optical CDMA, CULP CDMA, channel coding, optical networks, and information theory.

Sahar M. Aghajanzadeh was born in 1981. She received the B.S. and M.S. degrees in electrical engineering from Sharif University of Technology, Tehran, Iran, in 2003 and 2006, respectively.

Since March 2004, she has been a Research Assistant with the Advanced Communication Research Institute, Wireless Research Laboratory of the Electrical Engineering Department, Sharif University of Technology. Her research interests include wireless communications, specifically wireless optical communications, free space optics, optical CDMA, channel coding, and information theory.

Masoumeh Nasiri-Kenari (S'90–M'94) received the B.S. and M.S. degrees from Isfahan University of Technology, Isfahan, Iran, in 1986 and 1987, respectively, and the Ph.D. degree from University of Utah, Salt Lake City, in 1993, all in electrical engineering.

From 1987 to 1988, she was a Technical Instructor and a Research Assistant with Isfahan University of Technology. Since 1994, she has been with the Department of Electrical Engineering, Sharif University of Technology, Tehran, Iran, where she is currently a Professor. She is also the Director with the Wireless Research Laboratory of the Electrical Engineering Department. From 1999 to 2001, she was a Codirector with the Advanced Communication Science Research Laboratory, Iran Telecommunication Research Center, Tehran. Her current research interests are in wireless communication systems, error-correcting codes, and optical communication systems.

Mahdi Karimi was born in 1982. He received the B.S. degree (with honors) in electrical engineering from Isfahan University of Technology, Isfahan, Iran, in 2004. He is currently working toward the M.S. degree in electrical engineering in Sharif University of Technology, Tehran, Iran.

Since March 2004, he has been a Research Assistant with the Advanced Communication Research Institute, Wireless Research Laboratory of the Electrical Engineering Department, Sharif University of Technology. His research interests include information theory and channel coding, optical communication systems, specifically optical CDMA, and CULP CDMA.